forum acusticum 2023

COMPARISON OF DIFFERENT SMA-BASED ADAPTIVE TUNED MASS DAMPERS

Stefano Manzoni[1] **Antonio Argentino**[1] **Marta Berardengo**[2*]
Francescantonio Lucà[1] **Marcello Vanali**[3]
[1] Department of Mechanical Engineering, Politecnico di Milano, Italy
[2] DIME, University of Genoa, Italy
[3] Department of Engineering and Architecture, University of Parma, Italy

ABSTRACT

The use of smart materials has proven to be an effective strategy in the development of adaptive tuned mass dampers. Among different possible materials, shape memory alloys show specific features which make their use advantageous for building adaptive tuned mass dampers. More in detail, by heating/cooling the shape memory alloy components, it is possible to change the natural frequency of the adaptive tuned mass damper, thus allowing maintaining the adaptive mass damper tuned on the primary system to be damped. The heating/cooling is obtained by changing the amount of electrical current flowing through the shape memory alloy elements and, consequently, the amount of heat produced through Joule's effect. This paper compares the two main layouts for designing adaptive tuned mass dampers based on shape memory alloys in case the primary system to be damped is excited by a disturbance of random nature: cantilever beams and tensioned wires with a central mass. The two layouts, which can be described through detailed and experimentally validated models, are compared in terms of adaptation capability, exerted force and electrical power consumption. It results that the wire-based layout, despite being characterised by a more complicated set-up, is less demanding in terms of power consumption and shows much better adaptation capability.

Keywords: tuned mass damper, adaptive tuned mass damper, shape memory alloys, vibration, damping

*__Corresponding author__: marta.berardengo@unige.it.

1. INTRODUCTION

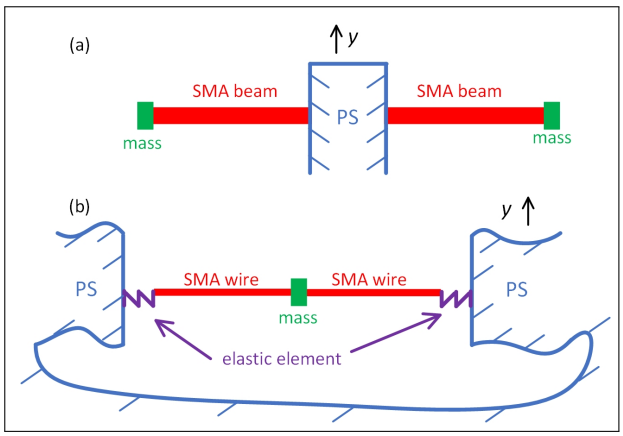

Figure 1. Layouts of the SMA-based ATMDs: beam-based (a) and wire-based (b). y is the displacement of the PS at the contact point with the ATMD.

Tuned mass dampers (TMDs) are devices for reducing vibrations in primary systems/structures (PS) (e.g., [1–3]). When TMD dynamic properties are tuned on the characteristics of the PS, they can often strongly reduce the vibration of the PS; the main problem with the employment of TMDs is that the vibration reduction can be impaired when incorrect tuning occurs (e.g., if a mistuning, due to shifts of the environmental variables, occurs). To avoid mistuning, many researchers have developed adaptive tuned mass dampers (ATMDs) able to change their dynamic properties in response to external

stimuli (e.g., [4–6]) so that perfect tuning can be recovered. Among the different possibilities for developing ATMDs (e.g., [7, 8]), the use of shape memory alloys (SMA) is promising. The main layouts of ATMDs relying on SMA elements are: (i) cantilever beams (e.g., [9, 10]) and (ii) wires with a central mass (e.g., [11]) (additional masses can be also used for multimode control [12]); see Fig. 1. Note that the beam-based layout is here built by employing two beams in order to have just a vertical force on the PS, avoiding torques (see Fig. 1a). For both the ATMD layouts, the SMA elements are heated and cooled by varying the current i flowing through them. Both types can significantly reduce PS vibrations, but there are few studies in the literature comparing them. This comparison, which is the main objective of the paper, will be made in terms of the following aspects:

- adaptation capability which indicates the extent to which the natural frequencies of the ATMD can be changed. In case also damping has to be tuned, both the layouts can be easily combined with additional devices (e.g., eddy current devices [11]) for damping tuning;
- force applied by the ATMD on the PS, which is in relation to the achievable vibration reduction performance;
- power consumption due to the need to apply current to the SMA elements to adapt the ATMD natural frequency.

The structure of the manuscript is the following: Section 2 gives a description of ATMD operating principles and modeling methods; Section 3 presents the experimental tests conducted to demonstrate the effectiveness of the adaptability of the ATMDs, and Section 4 compares beam-based and wire-based ATMDs employing the aforementioned models.

It is noticed that the authors of this paper previously published other papers on the use of SMA elements for building ATMDs, treating different topics, e.g., from mono-modal tuning [11] to multi-mode tuning [12] of wire-based ATMDs. Recently, they also compared wire- and beam-based SMA ATMDs in [13]. The present manuscript aims at giving an overview of the main results and approaches for describing SMA-based ATMDs.

2. WORKING PRINCIPLES AND MODELING APPROACHES OF THE ATMDS

This section describes the operating principles and modeling methods of the two ATMDs for linking the input current i to the frequency response function (FRF) of the resulting ATMD. Beam ATMDs are discussed in Section 2.1 and wire ATMDs in Section 2.2.

2.1 Beam-based ATMD

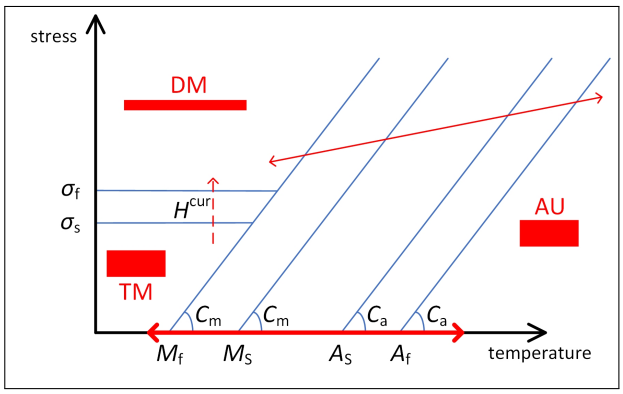

Figure 2. Temperature-stress plot for SMA elements.

The typical temperature-stress diagram of SMA elements [14] is presented in Fig. 2. The operating principle of this ATMD can be explained as follows: by changing temperature in the absence of stress, it is possible to pass from Twinned Martensite (TM) to Austenite (AU) and vice versa (see red thick solid double arrow in Fig. 2). Having the SMA element the same geometry in AU and TM, the main change in the SMA elements is in the value of the Young's modulus. Thanks to this, the natural frequency of the SMA beam is changed by changing its temperature T and the change of T is obtained by changing the value of i. The model describing this ATMD is made up of three different sub-models that are then grouped in order to find the relation between the input current i and the FRF of the ATMD [13]. More precisely, the FRFs considered here are that between the displacement Y of the PS at the contact point and the displacement Z of a given point of the beam (indicated as G_{ZY}) and that between Y and the force S exerted by the ATMD on the PS (referred to as G_{SY}). The three sub-models are a thermal model, a material model and a dynamic model. More details about them and how to gather them are available in [13].

2.2 Wire-based ATMD

SMA material faces a phase transformation also by applying a stress over σ_f at environmental temperature (see Fig. 2) and then changing temperature. This allows passing from detwinned martensite (DM) to AU and vice versa (see the thin red solid double arrow in Fig. 2). This double arrow does not mean that the temperature–stress states experienced by the SMA element are the same in both the directions of transformation, but only that a change of stress occurs when temperature is changed. The natural frequency variation is mainly related to the change of shape (between AU and DM), even if also material parameters change. Therefore, an ATMD can be built with an oscillating SMA wire with a central mass exploiting the mentioned way to change SMA shape. The SMA wire must be pre-stressed over σ_f by employing elastic elements (see Fig. 1b). These elements also allow linking the wire to the PS. As in the case of beam-ATMD, the change of current i flowing in the SMA elements allows changing the temperature of the SMA element.

Also in this case, three sub-models (i.e., thermal, material and dynamical) are grouped with the aim of achieving the link between the value of i and the previously mentioned FRFs. In this case, the global model is more complicated than the one of the beam-ATMD, mainly because of the change of stress into the wire and of wire shape (i.e., length) during the transformations. Details about these models are available in [13].

3. EXPERIMENTAL TESTS

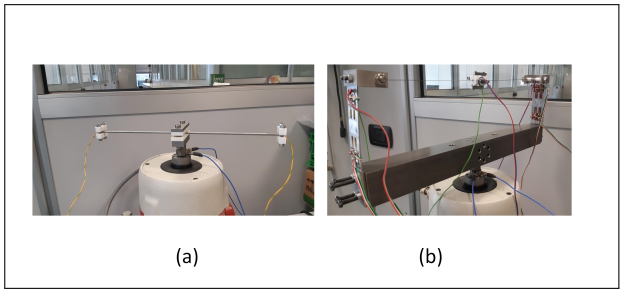

Figure 3. Experimental set-ups: beam-ATMD (a) and wire-ATMD (b).

Experimental tests were carried out for giving evidence to the working principles of the ATMDs. The set-ups used are shown in Fig. 3 (see [13] for more details).

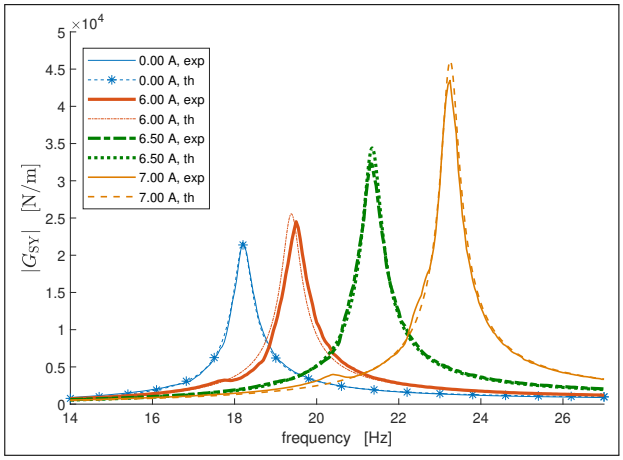

Figure 4. Experimental (exp) and theoretical (th) amplitudes of FRFs G_{SY} for the beam-ATMD while heating.

Figure 4 evidences the satisfactory match between experimental and model FRFs for the beam-ATMD and similar results were obtained for the wire-ATMD. The comparison presented in the figure is related to the FRFs between Y and S for different values of i.

For both the ATMDs, a higher natural frequency value can be obtained with a lower temperature (and, therefore, a lower current i) when cooling compared to heating (see Fig. 5 for the wire-ATMD, as an example). Indeed, the threshold temperatures for the start of the transformation from TM/DM to AU are larger compared to the corresponding ones related to the transformation from AU to TM/DM (see Fig. 2). More tests and results can be found in [13].

4. ATMD COMPARISON

This section compares the wire- and beam-ATMD. The nominal data employed for the comparisons are gathered in Table 1. In all the comparisons presented in the next subsections, the two ATMDs are designed such that they have the first natural frequency ω_1 at 30π rad/s at environmental temperature (i.e., i=0 A). Moreover, the global mass M_{tot} of the ATMDs is kept equal in all the comparisons in order to have the same weight for the two devices. It is noticed that the value of M_{tot} is the sum of the mass of the wire/beam plus the additional concentrated masses (see Fig. 1). Furthermore, the following data have been assumed for the comparisons: wire diameter equal to 0.5

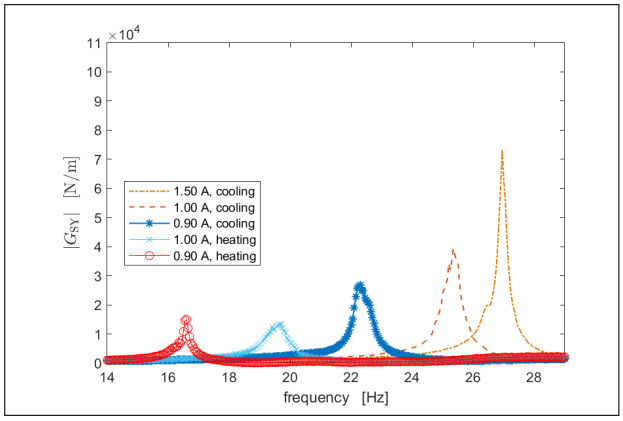

Figure 5. Experimental amplitudes of FRFs G_{SY} for the wire-ATMD while either heating or cooling the SMA wire.

mm and beam with circular hollow section characterized by an outer diameter of 4 mm and a thickness of 0.5 mm. The stiffness of the elastic elements for the wire layout evidenced in Fig. 1b was set such that the stress value into the wire was equal to 50 MPa in DM at environmental temperature and 200 MPa in AU. The interested reader can find more details and results about the comparisons in [13].

4.1 Comparison in terms of adaptation capability

The change of the first natural frequency for the wire-ATMD is approximately ten times larger than for the beam-ATMD and such a result is mostly the same for all the considered M_{tot} values, which ranged between 0.02 and 0.30 kg. The reason for such a large difference is related to the different mechanisms exploited in the two ATMD types for adjusting the ATMD natural frequency. In beam-ATMDs, the main mechanism influencing the natural frequency value is the change of Young's modulus from TM to AU and vice versa. Conversely, in wire-ATMDs, the change of shape of the wire from DM to AU, and vice versa, implies a change of tensioning force in the wire due to the elastic elements (see Fig. 1b). This second mechanism allows achieving a much larger eigenfrequency change compared to the first mechanism for usual values of the parameters of SMA elements.

Table 1. Parameter values for both SMA beams and wires used for the comparisons. See [13] for the definition of all the symbols.

Parameter	Value
A_{s} [°C]	68.6
A_{f} [°C]	78.9
M_{s} [°C]	55.2
M_{f} [°C]	42.7
C_{A} [MPa/°C]	9.90
C_{M} [MPa/°C]	6.83
H^{cur} [-]	$4.39{\cdot}10^{-2}$
α [°C^{-1}]	10^{-6}
E_{m} [GPa]	32.1
E_{a} [GPa]	39.5
ρ_{m} [Ωm]	$90{\cdot}10^{-8}$
ρ_{a} [Ωm]	$100{\cdot}10^{-8}$

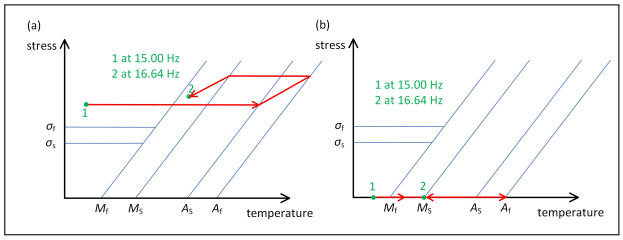

Figure 6. Heating/cooling paths considered for the comparisons: wire-ATMD (a) and beam-ATMD (b).

4.2 Comparison in terms of force exerted on the PS

The range of the natural frequency covered by the beam-ATMD is the starting point for this analysis because it is the layout with narrower range of frequency adaptation (see Section 4.1), varying from $\omega_1^{\mathrm{M,beam}}$ to $\omega_1^{\mathrm{A,beam}}$ (the superscript M indicates that the SMA element is in martensite at environmental temperature and the superscript A indicates that the SMA element has been heated and it is in AU phase). The wire-ATMD can be tuned correspondingly (see below). In the case considered here, $\omega_1^{\mathrm{M,beam}}$=30$\pi$ rad/s (i.e., 15 Hz) (see previously) and $\omega_1^{\mathrm{A,beam}}$ results equal to about 33.28π rad/s (i.e., 16.64 Hz).

The wire is initially tuned to $\omega_1^{\mathrm{M,wire}}$ =

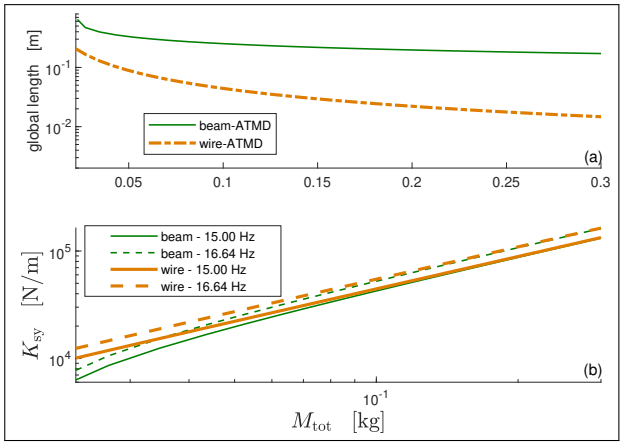

Figure 7. Trends of ATMD global length (a) and K_{sy} (b) as functions of M_{tot}.

$\omega_1^{\mathrm{M,beam}}$=30$\pi$ rad/s (i.e., 15 Hz) at environmental temperature (point 1 in Fig. 6a). Wire temperature T is then increased until achieving complete transformation in AU. Being $\omega_1^{\mathrm{A,wire}} > \omega_1^{\mathrm{A,beam}}$, the temperature of the wire is then decreased until $\omega_1^{\mathrm{wire}} = \omega_1^{\mathrm{A,beam}}$ (point 2 in Fig. 6a). The natural frequency value results equal to approximately 33.28π rad/s (i.e., 16.64 Hz, see previously). Therefore, the two ATMD layouts are compared at 15.00 (see points 1 in Figs. 6a and b) and 16.64 Hz (see points 2 in Figs. 6a and b).

The relation between the value of M_{tot} and the corresponding value of the global length at environmental temperature of the ATMD is shown in Fig. 7a. It is evident that the wire-ATMD is shorter than the beam-ATMD. This is also due to the different bending stiffness in beams and wires. Furthermore, Fig. 7b shows the peak values (i.e., the amplitude values at resonance) of the FRF G_{SY}, called K_{sy}. As expected from the results obtained in the experiments, these peaks become higher at higher frequency (compare the curves of different frequency values in the same plot). Furthermore, it is evident that beam- and wire-ATMDs exert similar forces on the PS when the value of M_{tot} increases, while higher forces are generated by the wire-ATMD for small values of M_{tot}. This difference at low M_{tot} values is probably also due to the fact that the global mass is mainly concentrated in the central mass for the wire-ATMD, while it is spread among the two concentrated masses and the beam in the case of the beam-ATMD.

4.3 Comparison in terms of electric power consumption

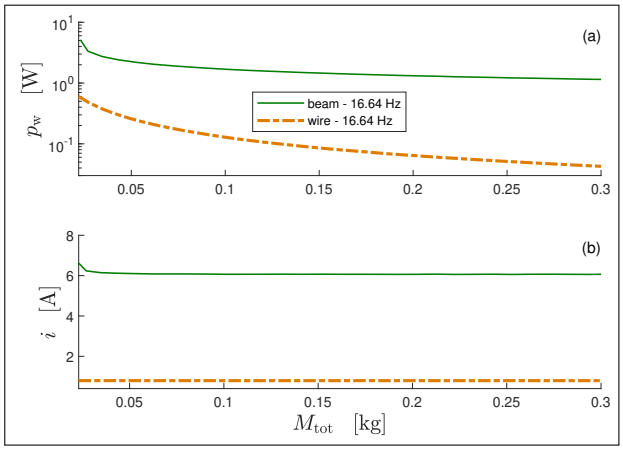

Figure 8. Trends of p_{w} (a) and i (b) as functions of M_{tot}.

This subsection compares the two ATMD layouts in terms of power p_{w} and current i needed to bring the ATMD at the maximum natural frequency value, that is 16.64 Hz in this case (see previously).

Figures 8a and b present the power p_{w} and the current i trends, respectively, as functions of the value of M_{tot}. The wire-ATMD is significantly less demanding in terms of electrical consumption. Often, the power consumption of the wire-ATMD is approximately ten times lower compared to that of the beam-ATMD.

5. CONCLUSION

The paper has addressed the comparison between the two main configurations for SMA-based ATMDs: wire-based and beam-based. Wire-ATMD results significantly less demanding in terms of power consumption, and it is also able to exert equal or larger forces compared to the beam-ATMD. Furthermore, its adaptation range is strongly larger compared to the beam-ATMD. However, all these advantages are balanced by a more complicated design layout because of the presence of elastic elements which are instead absent in the beam-ATMD.

6. REFERENCES

[1] J. Høgsberg, "Damping of coupled bending-torsion beam vibrations by a two-dof tmd with analogous cou-

pling," *Journal of Structural Dynamics*, no. 1, pp. 1–29, 2021.

[2] F. Santos and J. Nunes, "Toward an adaptive vibration absorber using shape-memory alloys, for civil engineering applications," *Journal of Intelligent Material Systems and Structures*, vol. 29, no. 5, pp. 729–740, 2018.

[3] S. Krenk and J. Høgsberg, "Equal modal damping design for a family of resonant vibration control formats," *Journal of Applied Mechanics*, vol. 19, no. 9, pp. 1294–1315, 2013.

[4] L. Wang, S. Nagarajaiah, Y. Zhou, and W. Shi, "Experimental study on adaptive-passive tuned mass damper with variable stiffness for vertical human-induced vibration control," *Engineering Structures*, vol. 280, 2023.

[5] M. Acar and C. Yilmaz, "Design of an adaptive–passive dynamic vibration absorber composed of a string–mass system equipped with negative stiffness tension adjusting mechanism," *Journal of Sound and Vibration*, vol. 332, no. 2, pp. 231–245, 2013.

[6] L. Zhang, L. Hong, J. S. Dhupia, S. Johnson, Z. Qaiser, and Z. Zhou, "A novel semi-active tuned mass damper with a continuously tunable stiffness," *Proceedings of the Institution of Mechanical Engineers, Part C: Journal of Mechanical Engineering Science*, vol. 237, pp. 281–293, 2023.

[7] G. M. Chatziathanasiou, N. A. Chrysochoidis, C. S. Rekatsinas, and D. A. Saravanos, "A semi-active shunted piezoelectric tuned-mass-damper for multimodal vibration control of large flexible structures," *Journal of Sound and Vibration*, vol. 537, p. 117222, 2022.

[8] F. Weber and M. Maślanka, "Frequency and damping adaptation of a TMD with controlled MR damper," *Smart Materials and Structures*, vol. 21, no. 5, p. 055011, 2012.

[9] E. Rustighi, M. J. Brennan, and B. R. Mace, "A shape memory alloy adaptive tuned vibration absorber: design and implementation," *Smart Materials and Structures*, vol. 14, no. 1, pp. 19–28, 2005.

[10] K. Williams, G. Chiu, and R. Bernhard, "Adaptive-Passive Absorbers Using Shape-Memory Alloys," *Journal of Sound and Vibration*, vol. 249, no. 5, pp. 835–848, 2002.

[11] M. Berardengo, A. Cigada, F. Guanziroli, and S. Manzoni, "Modelling and control of an adaptive tuned mass damper based on shape memory alloys and eddy currents," *Journal of Sound and Vibration*, vol. 349, pp. 18–38, 2015.

[12] M. Berardengo, G. Della Porta, S. Manzoni, and M. Vanali, "A multi-modal adaptive tuned mass damper based on shape memory alloys," *Journal of Intelligent Material Systems and Structures*, vol. 30, no. 4, pp. 536–555, 2019.

[13] S. Manzoni, A. Argentino, F. Lucà, M. Berardengo, and M. Vanali, "Sma-based adaptive tuned mass dampers: Analysis and comparison," *Mechanical Systems and Signal Processing*, vol. 186, 2023.

[14] D. Lagoudas, *Shape memory alloys: modeling and engineering applications*. Springer, 2008.